Redheffer products and numerical approximation of currents in one-dimensional semiconductor kinetic models

Laurent Gosse

REDHEFFER PRODUCTS AND NUMERICAL APPROXIMATION OF CURRENTS IN ONE-DIMENSIONAL SEMICONDUCTOR KINETIC MODELS

LAURENT GOSSE*

Dedicated to the memory of Naoufel Ben Abdallah (1968–2010)

Abstract. When numerically simulating a kinetic model of n^+nn^+ semiconductor device, obtaining a constant macroscopic current at steady-state is still a challenging task. Part of the difficulty comes from the multiscale, discontinuous nature of both $p|n$ junctions which create spikes of electric field and enclose a channel where corresponding depletion layers glue together. The kinetic formalism furnishes a model holding inside the whole domain, but at the price of strongly-varying parameters. By concentrating both the electric acceleration and the linear collision terms at each interface of a Cartesian computational grid, we can treat them by means of a Godunov scheme involving 2 types of scattering matrices. Combining both these mechanisms into a global S-matrix can be achieved thanks to "Redheffer's star-product". Assuming that the resulting S-matrix is stochastic permits to prove maximum principles under a mild CFL restriction. Numerical illustrations of collisional Landau damping and various n^+nn^+ devices are provided on coarse grids.

Key words. Discrete ordinates; Case's elementary solutions; Hamiltonian-Preserving scheme; Kinetic model of semiconductors; Redheffer star-product; Scattering matrix; Well-Balanced scheme.

AMS subject classifications. 65M06, 82D37.

1. Introduction and preliminaries. Our main goal is to compute a reliable numerical kinetic density of mobile charge carriers (either electrons or holes) in the vicinity of a $p|n$ junction represented on an interface of the 1D computational grid. The following simplifying assumptions are made throughout this text:

1. carriers recombination is not modeled, we treat only one equation rendering for the dynamics of the majority carriers (*i.e.* electrons),
2. the dielectric value is depends on impurity concentration (*i.e.* doping),
3. the carriers mobility can depend on both the doping and the electric field.

Numerical issues come from the subtle balance occurring around a $p|n$ junction:

- conduction electrons from donors (resp. holes for acceptors) first are attracted by opposite ions, hence diffuse out of the n (resp. p) area,
- until the negative ionization of acceptors (resp. positive ionization of donors) creates a potential barrier stopping this motion.
- This "spiky" electric field is supported inside a limited region, located around the junction, where electrons (holes) aren't available for current conduction.

It is called a "depletion layer", its length depends on impurity concentration and applied voltage: this area can be identified as an intrinsic semiconductor. The channel of a n^+nn^+ device gets filled with carriers until depletion layers corresponding to both the forward bias and the specificities of the junctions are correctly created and merged.

1.1. The relaxation-time approximation (RTA) kinetic model. A derivation of the "RTA approximation" of the low-density quadratic collision term of Vlasov-Boltzmann (also called Boltzmann-Poisson) equation is presented in [38], pages 85-86. Here, following [15], we simplify further this multi-D weakly nonlinear kinetic equation by restricting our study to simplified devices in one dimension by assuming that

*IAC–CNR "MAURO PICONE" (SEZIONE DI ROMA), VIA DEI TAURINI 19, 00185 ROME (ITALY) L.GOSSE@BA.IAC.CNR.IT

most of the salient features of the electronic transport are given in the direction parallel to the force field induced by Poisson's potential. Hence we are led to considering the following kinetic equation, already scrutinized in [33], Chapters 11 and 15:

$$\partial_t f + v\partial_x f + E\partial_v f = \frac{1}{\tau(x)}\left(\mathcal{M}_\theta(v)\int_{\mathbb{R}} f(t,x,v')dv' - f\right), \quad t,v \in \mathbb{R}_*^+ \times \mathbb{R}, \quad (1.1)$$

where $f(t,x,v)$ stands for the kinetic density depending on a time, space and velocity variables, τ is a relaxation time and $E(t,x) = -\partial_x\varphi(t,x)$ is the electric field given by:

$$-\lambda^2(x)\partial_{xx}\varphi = \rho - \rho_D(x), \qquad \rho(t,x) = \int_{\mathbb{R}} f(t,x,v)dv. \quad (1.2)$$

The parameter $\lambda^2 > 0$ is the scaled Debye length which renders the electrons screening distance in the material and $\rho_D(x) > 0$ is the doping profile, *i.e.* the concentration of donor impurities molten in the semiconductor crystal. Generally, the equations (1.1), (1.2) are set in a bounded space domain, $x \in (-1,1)$ and boundary conditions read:

$$f(t,x=\mp 1,\pm|v|) = \rho_D(\mp 1)\mathcal{M}_\theta(v), \quad \varphi(t,x=-1) = 0, \quad \varphi(t,x=1) = -V, \quad (1.3)$$

$$\mathcal{M}_\theta(v) = \frac{1}{\sqrt{2\pi\theta}}\exp(-\frac{v^2}{2\theta}), \qquad v \in \mathbb{R},$$

being the Maxwellian distribution at the lattice temperature $\theta > 0$ and $V > 0$ a voltage bias. Such inflow boundary data render ohmic contacts at each device's edge. It's essentially the model advocated in *e.g.* [12, 15] and studied theoretically in [13, 27].

1.2. Overview of the "elementary solutions" literature. According to *e.g.* [2], a main goal when it comes to performing numerical simulations of the aforementioned weakly nonlinear system is the determination of the so–called "Current-Voltage relation", that is to say the (constant) macroscopic flow $J(t,x) = \int_{\mathbb{R}} vf(t,x,v)dv$ at steady-state expressed as a function of the biasing value V. Clearly, this asks for a numerical method which is able to stabilize in large times onto a stationary kinetic density $\bar{f}$ endowed with a constant moment of order 1: see [11] for theoretical details. Such a requirement is reminiscent of the so–called "well-balanced property" for shallow water equations, for which one seeks numerical stationary flows endowed with a constant discharge, even in presence of a strongly-varying topography term [14].

This leads to the question about extending the well-balanced framework from quasi-linear hyperbolic systems of balance laws toward collisional kinetic equations: instead of localizing a topography term at each interface of a Cartesian computational grid, one is now led to (formally) concentrate, by means of Dirac masses [29], both the collision process, and the Vlasov acceleration term as well. The handling of linear collisional processes in a kinetic time-dependent setup is described in [30, 31, 32] and reviewed in Part II of [33]: it consists in building at each interface a "scattering matrix" which relates the incoming states $f_{j-1}^n(|v|), f_j^n(-|v|)$ to a set of outgoing ones, $\tilde{f}_{j-\frac{1}{2}}^n(\pm|v|)$, *cf.* [28] and Fig. 2.1. This scattering matrix is usually obtained from the exact integration of the stationary equations (more astute manners exist, see [9]).

In the context of 1+1-dimensional linear kinetic models, this immediately raises the issue of deriving exact solutions of boundary-value problems for the corresponding stationary equations: such a program was thoroughly studied after Case's influential paper [16] on "elementary solutions", see *e.g.* [1, 7, 17, 18, 39] which can be presented

as "spectral Green's functions" [5]. Thanks to Siewert's works [3, 4, 47], this was converted into a numerical algorithm, originally designed for steady-state computations involving least-square procedures, referred to as "Analytical Discrete-Ordinates". The extension to unsteady equations was first performed in [30] just by observing that the well-balanced approach is equivalent to concentrating the scattering process of collisions at each interface of the grid: this led to high-quality numerical results for various models [33]. One shortcoming at this stage was the difficulty of including a Vlasov-type acceleration term: indeed, several authors tried to derive a set of "elementary solutions" for simple models of collisional Vlasov equations, see [21, 42, 49]. Unfortunately, left apart the special case of Vlasov-Fokker-Planck models (see [33], Chapters 12-13), these spectral solutions were far too intricate to be used for producing an efficient numerical routine. An alternative construction was set up in [33], Chapter 11, and led to an efficient algorithm partially built on a high-field asymptotic distribution [26, 12]. However, this derivation may be felt as somewhat rigid because such an asymptotic density is rarely exactly computable. A remedy may consist in "marrying" both the exact resolutions of a Vlasov equation by means of the Hamiltonian-Preserving method, see [37] also [10, 34], which can be rephrased as the action of a local (stochastic) scattering matrix and a linear collisional one. An issue is that one doesn't obtain a scattering matrix out of the matrix product of two of them; the key is to consider instead the **Redheffer's star-product**, [44, 48].

1.3. Organization of the paper. Our main objective is to describe a practical algorithm which combines the nice properties of both the Hamiltonian-Preserving (HP) treatment of the Vlasov acceleration term [37, 50] and the scattering matrices obtained through the so–called Analytical Discrete-Ordinates (ADO) method [3, 4, 47], thanks to the Redheffer product of scattering matrices, in the formulation of [48]. The paper is organized as follows: §2 is devoted to the derivation of the scattering matrices corresponding to the linear collision process (see §2.1) and the electric acceleration (see §2.2), respectively. The Redheffer product is presented in §3, together with a simple fix to ensure current preservation at the interfaces (see §3.2). A maximum principle for the resulting Godunov scheme is deduced in Proposition 1 (see §3.3). The drifted-Maxwellian simplification for handling source and drain heavily doped regions is recalled in §4, together with a correct manner to implement inflow boundary conditions. Then, in §5, some numerical results are provided at numerical steady-state in presence of discontinuous parameters. In §6, a more involved situation, where the relaxation parameter τ depends also on the electric field in order to render pinching effects and mobility saturation is studied. After concluding remarks delivered in §7, an Appendix A displays a short numerical study of weakly collisional Landau damping, following [22] (and [33], pages 225–227).

2. Scattering matrices for acceleration and collisions. Before entering the matters core, let us state a few relevant notions of linear algebra:

Definition 1. *A $N \times N$ real matrix M is called* stochastic *(or "Markov matrix") if all its entries are non-negative and the sum of each line's components equals 1:*

$$\forall 1 \leq i \leq N, \qquad \sum_{j=1}^{N} M_{i,j} = 1.$$

Lemma 2.1. *Let the $N \times N$ real matrix M be stochastic, then:*

1. *it preserves non-negativity,*

2. 1 is an eigenvalue associated to $\mathbf{1} := (1, 1, ..., 1) \in \mathbb{R}^N$,
3. $\|M\|_\infty = 1$.

Proof. Consider any $X \in \mathbb{R}^N_+$, the i^{th} component of MX is $\sum_{j=1}^N M_{i,j}X_j$ which is non-negative as a sum of non-negative terms (any line of M realizes a convex combination). If $X = \mathbf{1}$, any component of MX reads $\sum_{j=1}^N M_{i,j} = 1$ hence $\mathbf{1}$ is the eigenvector associated to the eigenvalue 1. Lastly, for any $X \in \mathbb{R}^N$ with $\|X\|_\infty = 1$, the i^{th} component of MX satisfies $\sum_{j=1}^N M_{i,j}X_j \leq \sum_{j=1}^N M_{i,j}|X_j| \leq 1$. Then $\|M\|_\infty \leq 1$ and since 1 is eigenvalue associated to $\mathbf{1}$, $\|M\|_\infty = 1$. □

2.1. Scattering matrix for linear (RTA) collision term. Hereafter, we are given a Cartesian computational grid in t, x determined by the positive parameters $\Delta t, \Delta x$; the shorthand notation is used, $x_j = j\Delta x$, $t^n = n\Delta t$, the control cell located around x_j is $C_j = (x_{j-\frac{1}{2}}, x_{j+\frac{1}{2}})$. Moreover, a maximal value of the velocity modulus is fixed, $v_{MAX} > 0$ and an even (Gaussian) quadrature is set on the interval $(-1, 1)$. As it is symmetric and 0 doesn't belong to it, it can safely be multiplied by v_{MAX},

$$\{v_k, \omega_k\}_{k=1,...,2K}, \qquad v_k = -v_{2K+1-k} \neq 0, \quad \omega_k = \omega_{2K+1-k}, \qquad K \in \mathbb{N}. \tag{2.1}$$

The shorthand notation will be used frequently:

$$\mathbf{V} = \{v_k\}_{k=K+1,...,2K} \in (0, v_{MAX})^K \qquad \mathbf{\Omega} = \{\omega_k\}_{k=K+1,...,2K} \in \mathbb{R}^K_+.$$

The numerical schemes advocated in Part II of [33] hinge on deriving a Godunov scheme for the "localized equation" which reads, when only collisions are included:

$$\partial_t f + v\partial_x f = \frac{\Delta x}{\tau} \sum_{j\in\mathbb{Z}} \left(\mathcal{M}_\theta(v) \int_{\mathbb{R}} f(t, x, v')dv' - f \right) \delta(x - x_{j-\frac{1}{2}}).$$

This is essentially the approach suggested in [29]: the presence of this "localized source term" induces a static discontinuity at each interface separating 2 control cells C_{j-1} and C_j and implies that the Godunov scheme reads, for each $0 < v_k \in \mathbf{V} \subset \mathbb{R}^K_+$:

$$\begin{aligned} f_j^{n+1}(v_k) &= f_j^n(v_k) - \tfrac{\Delta t}{\Delta x} v_k \left(f_j^n(v_k) - \tilde{f}^n_{j-\frac{1}{2}}(v_k) \right), \\ f_j^{n+1}(-v_k) &= f_j^n(-v_k) + \tfrac{\Delta t}{\Delta x} v_k \left(\tilde{f}^n_{j+\frac{1}{2}}(-v_k) - f_j^n(-v_k) \right). \end{aligned}$$

Let S_τ stand for the scattering matrix which relates incoming/outgoing states at each interface $x_{j-\frac{1}{2}}$: the former numerical scheme rewrites in a less usual way,

$$\begin{pmatrix} f_j^{n+1}(\mathbf{V}) \\ f_{j-1}^{n+1}(-\mathbf{V}) \end{pmatrix} = \left(1 - \mathbf{V}\frac{\Delta t}{\Delta x} \right) \begin{pmatrix} f_j^n(\mathbf{V}) \\ f_{j-1}^n(-\mathbf{V}) \end{pmatrix} + \mathbf{V}\frac{\Delta t}{\Delta x} S_\tau \begin{pmatrix} f_{j-1}^n(\mathbf{V}) \\ f_j^n(-\mathbf{V}) \end{pmatrix}. \tag{2.2}$$

The presentation is now centered on each interface $x_{j-\frac{1}{2}}$ of the grid (like in [23]), instead of the former one which is centered on each cell C_j. Observe that, since $0 < v_k \in \mathbf{V}$, the states $f_{j-1}^n(v_k), f_j^n(-v_k)$ **approach** in the sense of Glimm [28] the Dirac mass located at $x_{j-\frac{1}{2}}$. Previous experience implies that the entries of the scattering matrix are known from the solving of the (forward/backward) boundary-value problem with inflow data for the stationary equation of the original problem,

$$v\partial_x \bar{f} = \frac{1}{\tau} \left(\mathcal{M}_\theta(v) \int_{\mathbb{R}} \bar{f}(x, v')dv' - \bar{f} \right), \qquad x \in (0, \Delta x).$$

Now, since $\|\mathcal{M}_\theta\|_{L^1(\mathbb{R})} = 1$, it is known from [1, 18] that if $\bar{g}(x,v)$ solves a similar equation, namely $v\partial_x\bar{g} = \int_{\mathbb{R}} \mathcal{M}_\theta(v')\bar{g}(x,v')dv' - \bar{g}$, then $\bar{f}(x,v) = \mathcal{M}_\theta(v)\bar{g}(\frac{x}{\tau},v)$.

Solving the forward/backward problem for this last equation is easy according to Case's theory of "elementary solutions" that we don't recall; we refer instead to [6, 7, 16, 17, 39]. According to [3, 4, 47], one can derive the $2K \times 2K$ matrix S_τ by:

1. determining the eigenmodes ν_k (sometimes called "constants of separation") by considering the approximate stationary equation in the following form,

$$v\partial_x\bar{f}(x,v) + \bar{f}(x,v) = \int_0^{v_{MAX}} \mathcal{M}_\theta(v')\left[\bar{f}(x,v') + \bar{f}(x,-v')\right]dv'. \qquad (2.3)$$

Analogously with the continuous case, the separation variable ν is introduced:

$$\bar{f}(x,v) = \varphi(\nu,v)\exp(-x/\nu).$$

Plugging into (2.3) and taking the quadrature rule into account yields:

$$\left(1 \mp \frac{v_k}{\nu_k}\right)\varphi(\nu,\pm v_k) = \sum_{\ell=1+K}^{2K} \omega_\ell \mathcal{M}_\theta(v_\ell)\Big(\varphi(\nu,v_\ell)+\varphi(\nu,-v_\ell)\Big), \quad k \in \{1,...,K\}.$$

We denote $\Phi_\pm(\nu) = \varphi(\nu,\pm v_k)_{k\in\{1+K,\dots,2K\}}$ thus an eigenvalue problem arises:

$$\pm\frac{\mathbf{V}}{\nu}\Phi_\pm(\nu) = \Phi_\pm(\nu) - (\mathbf{\Omega}\mathcal{M}_\theta(\mathbf{V}))\otimes\Phi_\pm(\nu) - (\mathbf{\Omega}\mathcal{M}_\theta(\mathbf{V}))\otimes\Phi_\mp(\nu). \quad (2.4)$$

In [4, 47], Barichello, Siewert and Wright present an astute manner to recast this eigenvalue problem into a simpler formulation, which allows to prove the "interlacing property": $0 < v_1 < \nu_1 < v_2 < \nu_2 < ... < v_K < \nu_K$.

2. assembling the matrices $M, \tilde{M}$ based on the "elementary solutions". Since $\bar{g}(x,v) = 1, x - v$ are obviously solutions associated to the zero-eigenvalue, one deduces that $\bar{f}(x,v) = \mathcal{M}_\theta(v), \mathcal{M}_\theta(v)(\frac{x}{\tau} - v)$ are too (they are sometimes called "linear diffusion solutions" [25]). The other solutions are associated with finite eigenmodes: $\bar{g}(x,v) = \frac{\exp(-x/\nu)}{1-v/\nu}$, thus $\bar{f}(x,v) = \frac{\mathcal{M}_\theta(v)}{1-v/\nu}\exp(-\frac{x}{\tau\nu})$.

$$\bar{f}(x,\pm v_k) \simeq \mathcal{M}_\theta(v_k)\left[\alpha + \beta\left(\frac{x}{\tau} \mp v_k\right) + \mathcal{E}\left(\frac{x}{\tau},\pm v_k,\nu\right)\right], \quad v_k \in \mathbf{V}.$$

$\mathcal{E}$ is a finite superposition of damped modes involving ν, the "Knudsen layers":

$$\mathcal{E}(x,v,\nu) = \sum_{\ell=1}^{K-1}\left(\frac{A_\ell}{1-v/\nu_\ell}\exp(-x/\nu_\ell) + \frac{B_\ell}{1+v/\nu_\ell}\exp(x/\nu_\ell)\right). \qquad (2.5)$$

In order to compute the $2K$ outgoing states $\bar{f}(\Delta x, v_k), \bar{f}(0,-v_k)$, $v_k \in \mathbf{V}$, we must first deduce the set of $2K$ coefficients α, β, A, B from the supplied boundary data $\bar{f}(0,v_k), \bar{f}(\Delta x,-v_k)$, and then exploit them to derive the sought values. This leads to inverting a $2K \times 2K$ matrix M depending on $\nu \in \mathbb{R}_+^{K-1}$

$$M = \begin{pmatrix} \left(1-\mathbf{V}\otimes\nu^{-1}\right)^{-1} & \mathbf{1}_{\mathbb{R}^K} & \left(1+\mathbf{V}\otimes\nu^{-1}\right)^{-1}\exp(-\frac{\Delta x}{\tau\nu}) & -\mathbf{V} \\ \left(1+\mathbf{V}\otimes\nu^{-1}\right)^{-1}\exp(-\frac{\Delta x}{\tau\nu}) & \mathbf{1}_{\mathbb{R}^K} & \left(1-\mathbf{V}\otimes\nu^{-1}\right)^{-1} & \frac{\Delta x}{\tau}+\mathbf{V} \end{pmatrix},$$

and to defining the complementary matrix:

$$\tilde{M} = \begin{pmatrix} \left(1-\mathbf{V}\otimes\nu^{-1}\right)^{-1}\exp(-\frac{\Delta x}{\tau\nu}) & \mathbf{1}_{\mathbb{R}^K} & \left(1+\mathbf{V}\otimes\nu^{-1}\right)^{-1} & \frac{\Delta x}{\tau}-\mathbf{V} \\ \left(1+\mathbf{V}\otimes\nu^{-1}\right)^{-1} & \mathbf{1}_{\mathbb{R}^K} & \left(1-\mathbf{V}\otimes\nu^{-1}\right)^{-1}\exp(-\frac{\Delta x}{\tau\nu}) & \mathbf{V} \end{pmatrix}.$$

3. if D stands for the $2K\times 2K$ diagonal matrix which entries are $\{\mathcal{M}_\theta(\mathbf{V}),\mathcal{M}_\theta(\mathbf{V})\}$,

$$S_\tau = (D\tilde{M})\ (DM)^{-1} \tag{2.6}$$

is the expression of the desired scattering S-matrix used in (2.2), see Fig. 2.1.

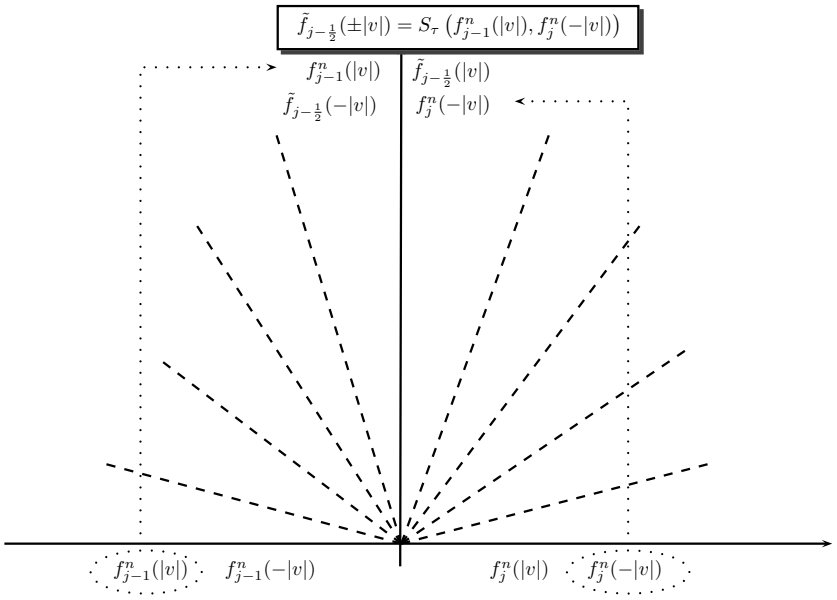

FIG. 2.1. *Riemann problem in the discrete ordinates and scattering matrix* S_τ

REMARK 1. *By defining another density* $g(t,x,v):=\frac{f(t,x,v)}{\mathcal{M}_\theta(v)}$, *(2.2)–(2.6) becomes*

$$\begin{pmatrix} g^{n+1}_j(\mathbf{V}) \\ g^{n+1}_{j-1}(-\mathbf{V}) \end{pmatrix} = \left(1-\mathbf{V}\frac{\Delta t}{\Delta x}\right)\begin{pmatrix} g^n_j(\mathbf{V}) \\ g^n_{j-1}(-\mathbf{V}) \end{pmatrix} + \mathbf{V}\frac{\Delta t}{\Delta x}\tilde{M}M^{-1}\begin{pmatrix} g^n_{j-1}(\mathbf{V}) \\ g^n_j(-\mathbf{V}) \end{pmatrix} \tag{2.7}$$

as one can easily check on a computer that for any $\tau,K>0$, *the product* $\tilde{M}M^{-1}$ *is stochastic. However, proving rigorously that this property holds uniformly in* τ,K *is an open problem, except for the simple case* $K=1$ *(see [33], Chapter 9, for details).*

2.2. Scattering matrix for the Vlasov acceleration term. The derivation of an approximation of the scattering matrix S_E for the linear Vlasov equation,

$$\partial_t f + v\partial_x f + E\partial_v f = 0, \qquad E\in\mathbb{R}, \tag{2.8}$$

follows exactly from the same ideas as before, except that it appears simpler as one doesn't need "elementary solutions". The exact solution of a inflow boundary-value (forward/backward) problem for the stationary equation, $v\partial_x\bar{f}+E\partial_v\bar{f}=0$ is given simply by "shifting velocities" as it is explained in [33, 34, 37, 50]. This construction (called "Scheme I" in [37]) furnishes a scattering matrix for Hamiltonian-Preserving by means of linear interpolation: numerical difficulties can arise because of the possibly weak variance of the probability density $\bar{f}$, see *e.g.* [46]. Once the $2K\times 2K$ matrix S_E is known, the numerical treatment of (2.8) simply consists in iterating (2.2) with S_E instead of S_τ. Hereafter, we recall how to construct S_E:

1. one first observes that it is enough to consider $E < 0$, because the stationary equation $v\partial_x \bar{f} + E\partial_v \bar{f} = 0$ is invariant if both v, E change signs. This means:

$$\begin{pmatrix} \tilde{f}^n_{j-\frac{1}{2}}(-\mathbf{V}) \\ \tilde{f}^n_{j-\frac{1}{2}}(\mathbf{V}) \end{pmatrix} = S_{-E} \begin{pmatrix} f^n_j(-\mathbf{V}) \\ f^n_{j-1}(\mathbf{V}) \end{pmatrix}.$$

2. assuming that $E < 0$, one loops on the indexes $k \in \{1, 2, ..., K\}$:
   - Let $v = \sqrt{(v_k)^2 - 2E\Delta x}$: $\tilde{k} = \max_\ell\{v_\ell \leq v\}$ and $\alpha_k = \frac{v - v_{\tilde{k}}}{v_{\tilde{k}+1} - v_{\tilde{k}}}$,

$$(S_E)_{k,\tilde{k}} = 1 - \alpha_k \qquad (S_E)_{k,\tilde{k}+1} = \alpha_k.$$

   - If $(v_k)^2 + 2E\Delta x \leq 0$, then $(S_E)_{K+k,k} = 1$.
   - Let $v = \sqrt{(v_k)^2 + 2E\Delta x}$, $\tilde{k} = \max_\ell\{v_\ell \leq v\}$, and $\alpha_{-k} = \frac{v - v_{\tilde{k}-1}}{v_{\tilde{k}} - v_{\tilde{k}-1}}$:

$$(S_E)_{K+k,K+\tilde{k}-1} = 1 - \alpha_{-k}, \qquad (S_E)_{K+k,K+\tilde{k}} = \alpha_{-k}.$$

3. The former linear interpolation doesn't systematically preserve neither the total mass nor the current. Another choice is to replace it by:

$$\alpha_k = \frac{\omega_k v_k - \omega_{\tilde{k}} v_{\tilde{k}}}{\omega_{\tilde{k}+1} v_{\tilde{k}+1} - \omega_{\tilde{k}} v_{\tilde{k}}} \qquad (S_E)_{k,\tilde{k}} = 1 - \alpha_k \qquad (S_E)_{k,\tilde{k}+1} = \alpha_k.$$

   The resulting matrix isn't always stochastic: it can contain negative entries. In the paper [37], the so–called "Scheme II" appears to be built in such a way so as to preserve the currents across the scattering process (see Fig 2.2). Its implementation seems quite heavy (see pages 294–296) though.

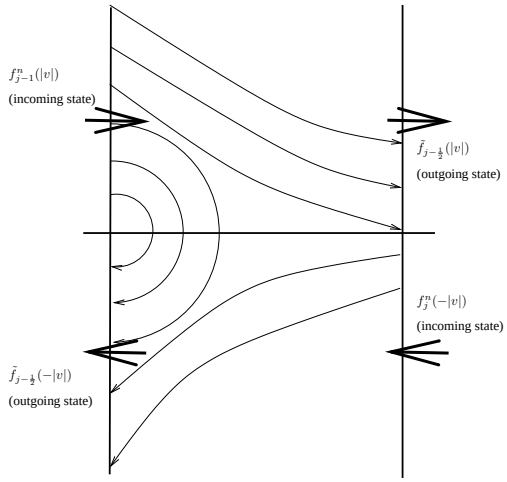

FIG. 2.2. *Illustration of the scattering process for Vlasov with* $E < 0$

2.3. Legendre polynomials and vanishing moments. Let us fix an interface $x_{j-\frac{1}{2}} \in \mathbb{R}$, and following *e.g.* [7], consider the incoming/outgoing states:

$$f_{in}(v) = \begin{pmatrix} f^n_j(-|v|) \\ f^n_{j-1}(|v|) \end{pmatrix}, \qquad f_{out}(v) = \begin{pmatrix} \tilde{f}_{j-\frac{1}{2}}(-|v|) \\ \tilde{f}_{j-\frac{1}{2}}(|v|) \end{pmatrix}.$$

By consistency with the stationary kinetic problem, we want mass conservation,

$$\sum_{k=1}^{2K} \omega_k \big(f_{in}(v_k) - f_{out}(v_k) \big) = 0, \tag{2.9}$$

(even if that is somewhat contradictory with working out Gaussian distributions in a bounded domain of the velocity variable) together with current preservation:

$$\sum_{k=1+K}^{2K} \omega_k v_k \left([f^n_{j-1}(v_k) - \tilde{f}_{j-\frac{1}{2}}(-v_k)] - [\tilde{f}_{j-\frac{1}{2}}(v_k) - f^n_j(-v_k)] \right),$$

$$\Leftrightarrow \qquad \sum_{k=1}^{2K} \omega_k |v_k| \big(f_{in}(v_k) - f_{out}(v_k) \big) = 0. \tag{2.10}$$

LEMMA 2.2. *Let* $\mathbf{V}' := \mathbf{V} - \frac{v_{MAX}}{2}$ *and* Id *be the identity, the modified S-matrix,*

$$\tilde{S}_E = S_E + \frac{1}{2v_{MAX}} \left\{ \mathbf{1} \otimes \begin{pmatrix} \mathbf{\Omega} \\ \mathbf{\Omega} \end{pmatrix} + \frac{12}{v^2_{MAX}} \begin{pmatrix} \mathbf{V}' \\ \mathbf{V}' \end{pmatrix} \otimes \begin{pmatrix} \mathbf{\Omega V}' \\ \mathbf{\Omega V}' \end{pmatrix} \right\} (Id - S_E),$$

enforces both mass and current preservations: (2.9), (2.10) hold for $f_{out} = \tilde{S}_E f_{in}$.

Proof. The equalities (2.9), (2.10) mean that $f_{in} - f_{out}$ has 2 vanishing moments against 1 and $|v|$. By linearity, such a property extends to any test function $\alpha + \beta|v|$, $\alpha, \beta \in \mathbb{R}^2$, too. Hence $f_{in} - f_{out}$ is orthogonal for the $L^2(-v_{MAX}, v_{MAX})$ scalar product to the plane spanned by $\{1, |v|\}$. Now, it is easy to see that,

$$\frac{1}{\sqrt{2v_{MAX}}}, \qquad \frac{\sqrt{6}(|v| - v_{MAX})}{v^{\frac{3}{2}}_{MAX}},$$

constitute an orthonormal basis of this plane. The least-squares solution,

$$f_{out} + \frac{1}{2v_{MAX}} \left(< f_{in} - f_{out}, 1 >_{L^2} + \frac{12v'}{v^2_{MAX}} < f_{in} - f_{out}, v' >_{L^2} \right),$$

for $v' := |v| - \frac{v_{MAX}}{2}$ has both the desired vanishing moments and is in Range$(\tilde{S}_E)$. □

REMARK 2. *The S-matrix formalism, suggested in [28, 29], is a manner to compute wave interactions in a very linearly degenerate framework: indeed, the Godunov scheme (2.2) inside a bounded domain can be seen as approximating a "lifted system",*

$$\partial_t f + v\partial_x f - \frac{1}{\tau(x)} \left(\mathcal{M}_\theta(v) \int_{\mathbb{R}} f(t,x,v')dv' - f \right) \partial_x a(x) = 0, \qquad \partial_t a(x) = 0,$$

where $a(x)$ *is a staircase function constant on* C_j*'s, and jumping of* Δx *at each interface* $x_{j-\frac{1}{2}}$ *(this jump yields a Dirac mass). When setting up the discrete-ordinates (2.1) in the* v *variable, we get a strictly hyperbolic* $(2K+1) \times (2K+1)$ *system where* $2K$ *characteristic fields are linear, and the last one is only linearly degenerate: the S-matrix gives the jump relations when the linear waves interact with the LD field.*

3. Combining acceleration and collisions with Redheffer product.

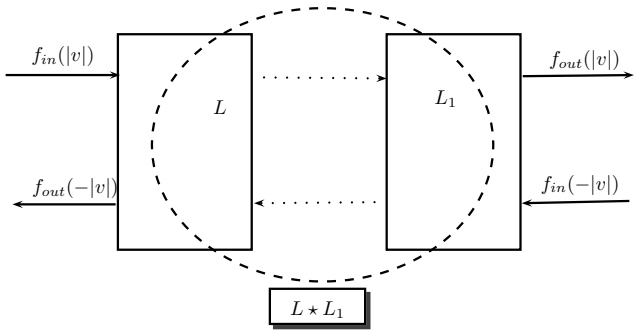

FIG. 3.1. *Illustration of Redheffer star-product*

3.1. Redheffer star-products of both scattering matrices. Now we have at hand all the elements to generate a scattering matrix for the linear problem,

$$\partial_t f + v\partial_x f + E^n_{j-\frac{1}{2}}\partial_v f = \frac{\Delta x}{\tau}\left(\mathcal{M}_\theta(v)\int_{\mathbb{R}} f(t,x,v')dv' - f\right)\delta(x - x_{j-\frac{1}{2}}),$$

with $E^n_{j-\frac{1}{2}} \in \mathbb{R}$, $\tau \in \mathbb{R}^+$, by computing $S_{\tau,E^n_{j-\frac{1}{2}}} = S_\tau \star S_{E^n_{j-\frac{1}{2}}}$ the "Redheffer product" [44] of the aforementioned matrices S_τ and $S_{E^n_{j-\frac{1}{2}}}$. Roughly speaking, it all amounts to a "space-splitting" algorithm, in which any two different scattering mechanisms are flanked infinitesimally close to one another. Following [48], we recall a definition of this "$\star$" product of 2 partitioned $2K \times 2K$ matrices L, L_1 (see Fig. 3.1):

$$L = \begin{pmatrix} A & B \\ C & D \end{pmatrix}, \qquad L_1 = \begin{pmatrix} A_1 & B_1 \\ C_1 & D_1 \end{pmatrix},$$

where both A, B, C, D and A_1, B_1, C_1, D_1 are sets of $K \times K$ matrices [40]. It reads:

$$L \star L_1 = \begin{pmatrix} A(Id - B_1C)^{-1}A_1 & B + A(Id - B_1C)^{-1}B_1D \\ C_1 + D_1C(Id - B_1C)^{-1}A_1 & D_1(Id - CB_1)^{-1}D \end{pmatrix}, \tag{3.1}$$

for Id standing for the $K \times K$ identity matrix. Obviously, for numerical efficiency, one must never implement the inverse of these $K \times K$ matrices, but instead perform simpler inversions of the resulting 2 linear systems. The Godunov scheme we propose for solving (1.1) is thus a slight modification of (2.2) which reads precisely:

$$\begin{pmatrix} f_j^{n+1}(\mathbf{V}) \\ f_{j-1}^{n+1}(-\mathbf{V}) \end{pmatrix} = \left(1 - \mathbf{V}\frac{\Delta t}{\Delta x}\right)\begin{pmatrix} f_j^n(\mathbf{V}) \\ f_{j-1}^n(-\mathbf{V}) \end{pmatrix} + \mathbf{V}\frac{\Delta t}{\Delta x}S^n_{j-\frac{1}{2}}\begin{pmatrix} f_{j-1}^n(\mathbf{V}) \\ f_j^n(-\mathbf{V}) \end{pmatrix}, \tag{3.2}$$

with the scattering matrix, partially deduced from a standard approximation of (1.2),

$$S^n_{j-\frac{1}{2}} := S_{\tau(x_{j-\frac{1}{2}})} \star S_{E^n_{j-\frac{1}{2}}}, \qquad E^n_{j-\frac{1}{2}} = -\frac{\varphi^n_j - \varphi^n_{j-1}}{\Delta x}. \tag{3.3}$$

We stress that, since the kinetic density $f^n_j(\pm\mathbf{V})$ is defined at each x_j, its moments are too, and consequently also the electric potential φ thanks to a standard second-order finite-difference algorithm. Hence the electric field, a first-order derivative of φ, is naturally computed at each interface $x_{j-\frac{1}{2}}$, and this is exactly what we want within

a "scattering perspective". Of course, the choice (3.3) is not unique: by analogy with second-order Strang's splitting in time, one may want to define instead

$$S^n_{j-\frac{1}{2}} := \left(S_{E^n_{j-\frac{1}{2}}/2} \star S_{\tau(x_{j-\frac{1}{2}})} \right) \star S_{E^n_{j-\frac{1}{2}}/2}, \tag{3.4}$$

thanks to the associativity of the $\star$-product, [48] (for a higher CPU cost, though). Such a symmetric S-matrix reveals itself useful for instance in computing accurately a n^+nn^+ device with zero bias imposed at both its edges. Since the scattering matrix S_E doesn't automatically generate outgoing states for which the macroscopic current is a constant, the scheme (3.2)–(3.3) may not stabilize correctly in large times: possible remedies are either the procedure presented in §2.3 or an even simpler fix below.

3.2. A simple fix to enforce current conservation. We explain now how one can proceed in order to recover a constant current across any interface $x_{j-\frac{1}{2}}$ in a cheap and robust manner. The Godunov scheme reads for $K = 1 + K, ..., 2K$:

$$\begin{aligned} f^{n+1}_j(v_k) &= f^n_j(v_k) - \tfrac{\Delta t}{\Delta x} v_k \left(f^n_j(v_k) - \tilde{f}^n_{j-\frac{1}{2}}(v_k) \right), \\ f^{n+1}_{j-1}(-v_k) &= f^n_{j-1}(-v_k) + \tfrac{\Delta t}{\Delta x} v_k \left(\tilde{f}^n_{j-\frac{1}{2}}(-v_k) - f^n_{j-1}(-v_k) \right), \end{aligned}$$

where, as shown in Fig. 2.1, $\tilde{f}^n_{j-\frac{1}{2}}(\pm\mathbf{V}) = S^n_{j-\frac{1}{2}}(f^n_{j-1}(-\mathbf{V}), f^n_j(-\mathbf{V}))$. Let $\delta \in \mathbb{R}$ stand for the possible macroscopic current defect, that is,

$$\delta := \sum_{0<v_k\in\mathbf{V}} \omega_k v_k \left[\left(f_{j-1}(v_k) + f_j(-v_k) \right) - \left(\tilde{f}_{j-\frac{1}{2}}(v_k) + \tilde{f}_{j-\frac{1}{2}}(-v_k) \right) \right]. \tag{3.5}$$

One must distribute this defect on both sides, $\tilde{f}_{j-\frac{1}{2}}(\pm\mathbf{V})$ in order to ensure that the macroscopic flow is constant across each interface: let $J_+ = \sum_{v_k\in\mathbf{V}} \omega_k v_k f_j(v_k)$ and $J_- = \sum_{v_k\in\mathbf{V}} \omega_k v_k f_{j-1}(-v_k)$, $0 \leq \alpha \leq 1$ then by modifying outgoing states like,

$$\tilde{f}^*_{j-\frac{1}{2}}(v_k) = \tilde{f}_{j-\frac{1}{2}}(v_k) + \frac{\delta\alpha}{J_+} f_j(v_k), \quad \tilde{f}^*_{j-\frac{1}{2}}(-v_k) = \tilde{f}_{j-\frac{1}{2}}(-v_k) - \frac{\delta(1-\alpha)}{J_-} f_{j-1}(-v_k),$$

one recovers two outgoing states $\tilde{f}^*_{j-\frac{1}{2}}(\pm v_k)$ such that the macroscopic current is constant across the discontinuity induced by the Dirac mass (which is essential for treating correctly the mass continuity equation). In practice, bypassing this slight correction of the scattered states of the kinetic equation prevents the numerical scheme to stabilize in large times onto an approximate kinetic density $f^n_j(\pm\mathbf{V})$ endowed with a flat macroscopic current (the flux term in the mass continuity equation).

We are left with a free parameter α, which value is fixed by mass conservation:

$$0 = \sum_{k=1+K}^{2K} \omega_k \left[\left(f_{j-1}(v_k) + f_j(-v_k) \right) - \left(\tilde{f}^*_{j-\frac{1}{2}}(v_k) + \tilde{f}^*_{j-\frac{1}{2}}(-v_k) \right) \right].$$

This constraint yields the following value: if $|\delta| > 0$,

$$\alpha = \frac{\displaystyle\sum_{k=1+K}^{2K} \omega_k \left[\frac{f_{j-1}(v_k) - \tilde{f}_{j-\frac{1}{2}}(v_k) + f_j(-v_k) - \tilde{f}_{j-\frac{1}{2}}(-v_k)}{\delta} + \frac{f_{j-1}(-v_k)}{J_-} \right]}{\displaystyle\sum_{k=1+K}^{2K} \omega_k \left[\frac{f_j(v_k)}{J_+} + \frac{f_{j-1}(-v_k)}{J_-} \right]}.$$

However, in the cases where, by construction, $S^n_{j-\frac{1}{2}}$ preserves the total mass,

$$\sum_{k=1+K}^{2K} \omega_k \left[f_{j-1}(v_k) - \tilde{f}_{j-\frac{1}{2}}(v_k) + f_j(-v_k) - \tilde{f}_{j-\frac{1}{2}}(-v_k) \right] = 0,$$

then the expression simplifies and finally one finds:

$$\alpha = \frac{\displaystyle\sum_{k=1+K}^{2K} \omega_k \left[\frac{f_{j-1}(-v_k)}{J_-} \right]}{\displaystyle\sum_{k=1+K}^{2K} \omega_k \left[\frac{f_j(v_k)}{J_+} + \frac{f_{j-1}(-v_k)}{J_-} \right]} \in [0,1]. \tag{3.6}$$

Notice that at numerical steady-state, velocity distributions match each other:

$$\tilde{f}^*_{j-\frac{1}{2}}(|v_k|) = f^n_j(|v_k|), \qquad \tilde{f}^*_{j-\frac{1}{2}}(-|v_k|) = f^n_{j-1}(-|v_k|).$$

In practice, the fix (3.6) can be set up even when the local scattering matrix $S^n_{j-\frac{1}{2}}$ doesn't exactly preserve the total mass, which is a rather stringent condition because one never has an infinite support in the v variable thus "tails" $|v_k| \simeq v_{MAX}$ are usually (slightly) flawed. Results of the forthcoming sections were obtained this way.

3.3. Stability of the resulting Godunov scheme. An interesting property of this method based on scattering S-matrices is its weak CFL criterion.

PROPOSITION 1. *Let $0 \leq f(t=0,x,v) \in L^\infty(\mathbb{R}^2)$ and assume both that,*

- *the mild CFL restriction $\Delta t \leq \Delta x / v_{MAX}$ holds,*
- *the S-matrix $S^n_{j-\frac{1}{2}}$ is stochastic for all $j, n \in \mathbb{Z} \times \mathbb{N}$.*

Then the Godunov scheme (3.2) is positivity-preserving and obeys to:

$$\forall j, n \in \mathbb{Z} \times \mathbb{N}, \qquad 0 \leq f^n_j(v_k) \leq \|f(t=0,\cdot,\cdot)\|_{L^\infty}. \tag{3.7}$$

Proof. We assume that initial data are sampled in such a manner that the L^∞ norm is preserved at time $n=0$. From Lemma 2.1, any matrix $S^n_{j-\frac{1}{2}}$ preserves the L^∞ norm and non-negativity: thus for any $j,k \in \mathbb{Z} \times \{1,...,2K\}$, $f^{n+1}_j(v_k) \geq 0$ as a sum of non-negative terms. Now, by using the presentation (2.2), it comes

$$\begin{aligned}
\left\| \begin{array}{c} f^{n+1}_j(\mathbf{V}) \\ f^{n+1}_{j-1}(-\mathbf{V}) \end{array} \right\|_\infty &= \max_k \left\{ \begin{array}{c} |f^{n+1}_j(v_k)| \\ |f^{n+1}_{j-1}(-v_k)| \end{array} \right\} \\
&= \max_k \left\{ \begin{array}{c} (1 - v_k \frac{\Delta t}{\Delta x}) |f^n_j(v_k)| + v_k \frac{\Delta t}{\Delta x} |\tilde{f}^n_{j-\frac{1}{2}}(v_k)| \\ (1 - v_k \frac{\Delta t}{\Delta x}) |f^n_{j-1}(-v_k)| + v_k \frac{\Delta t}{\Delta x} |\tilde{f}^n_{j-\frac{1}{2}}(-v_k)| \end{array} \right\} \\
&\leq (1 - v_{\bar{k}} \frac{\Delta t}{\Delta x}) \left\| \begin{array}{c} f^n_j(\mathbf{V}) \\ f^n_{j-1}(-\mathbf{V}) \end{array} \right\|_\infty + v_{\bar{k}} \frac{\Delta t}{\Delta x} \|S^n_{j-\frac{1}{2}}\|_\infty \left\| \begin{array}{c} f^n_{j-1}(\mathbf{V}) \\ f^n_j(-\mathbf{V}) \end{array} \right\|_\infty \\
&\leq (1 - v_{\bar{k}} \frac{\Delta t}{\Delta x}) \sup_{j',k} |f^n_{j'}(v_k)| + v_{\bar{k}} \frac{\Delta t}{\Delta x} \|S^n_{j-\frac{1}{2}}\|_\infty \sup_{j',k} |f^n_{j'}(v_k)| \\
&\leq \sup_{j',k} |f^n_{j'}(v_k)|.
\end{aligned}$$

The index $\bar{k}$ is the one for which the "max" is reached. This is enough to ensure that for all $j \in \mathbb{Z}$, there holds

$$\sup_{1\leq k\leq 2K} |f_j^{n+1}(v_k)| \leq \sup_{j'\in\mathbb{Z},\ 1\leq k\leq 2K} |f_{j'}^n(v_k)|,$$

and (3.7) follows by induction. □

For instance, Proposition 1 directly applies when setting up the matrix S_E derived in §2.2 in the context of Hamiltonian-Preserving approximations of linear Vlasov equations (which solutions are obtained by the method of characteristics, hence the maximum principle clearly holds). Such a uniform bound was obtained in [37] too, but here we show that it holds under a weaker CFL restriction. For kinetic equations endowed with linear relaxation, Proposition 1 applies to the modified scheme (2.7) in Remark 1: the obstacle is to prove rigorously that $\tilde{M}M^{-1}$ is stochastic for $K > 1$.

REMARK 3. *The bound (3.7) yields compactness in the weak-$\star$ topology. In the special case where the S-matrix is stochastic and depends only of time (not of space),*

$$\forall j \in \mathbb{Z}, \qquad S^n_{j-\frac{1}{2}} \equiv S^n,$$

then a L^∞ dissipation estimate holds for divided differences approximating $\frac{\partial^p f}{\partial x^p}(t,\cdot,\cdot)$, $p \in \mathbb{N}$ because the linear schemes (3.2), or (2.7), become invariant by x-translations.

4. Drifted-Maxwellian treatment of source and drain areas.

4.1. Computation of an approximate scattering matrix. For completeness, we hereafter recall quickly the algorithm presented in [33], pages 222-224. One argues that, since the hypothesis $f(t,x,v) \simeq \mathcal{M}_\theta(v)\rho(t,x)$ is used in deriving (1.1), see [38] page 84, the same procedure may allow to simplify the acceleration term in strongly doped areas: by approaching it with $E(t,x)\partial_v(\rho(t,x)\mathcal{M}_\theta(v))$, it comes,

$$\partial_t f + v\partial_x f = \frac{1}{\tau(x)}\left(\mathcal{M}_\theta(v)(1+v\frac{\tau E}{\theta})\int_{\mathbb{R}} f(t,x,v')dv' - f\right), \tag{4.1}$$

supplemented by (1.2) [42, 26]. The terminology "drifted Maxwellian" comes from:

$$\eta(v|E) := \left(1+v\frac{\tau E}{\theta}\right)\mathcal{M}_\theta(v) \simeq \exp\left(-\frac{v^2-2v\tau E}{2\theta}\right) \simeq \mathcal{M}_\theta(v-\tau E),$$

for $\tau|E| \ll 1$. It corresponds to a modeling where the motion of electrons is governed by the host medium's convection and scattering [42]. If $\tau|E|$ is small and the density of electrons has a velocity profile close to $\mathcal{M}_\theta(v-\tau E)$, a displaced Maxwellian determined by the temperature θ and the local drift velocity of the background medium, both models can be expected to yield similar results (and not far from the ones of the corresponding diffusion approximation) because even if the two kinetic equations describe two distinct physical processes, they share the same diffusion approximation.

At a given interface $x_{j-\frac{1}{2}}$, let's assume we know an average value $\bar{\rho}$ of the macroscopic density: the method of elementary solutions suggests an ansatz in the form,

$$\bar{f}(x,\pm v_k) \simeq \mathcal{M}_\theta(\pm v_k)\left[\alpha+\beta(\frac{x}{\tau}\mp v_k)+\mathcal{E}(\frac{x}{\tau},\pm v_k,\nu)+\bar{\rho}\frac{Ex}{\theta}\right], \quad v_k \in \mathbf{V},$$

where $E = E^n_{j-\frac{1}{2}}$ is the electric field, $\bar{\rho} = \bar{\rho}(f^n_{j-1}, f^n_j)$ is a local approximation of the macroscopic density, for instance, one may detect any spurious negative value with

$$\bar{\rho}(f^n_{j-1}, f^n_j) = \int_{\mathbb{R}} \sqrt{f^n_{j-1}(v)f^n_j(v)}dv,$$

$\mathcal{E}$ stands again for the damped modes (2.5). For a convenient choice of the coefficients, the expression is meant to match the incoming states:

$$\left.\begin{array}{rcl} \mathcal{M}_\theta(v_k)[\alpha-\beta v_k+\mathcal{E}(0,v_k,\nu)] & = & f^n_{j-1}(v_k), \\ \mathcal{M}_\theta(-v_k)\left[\alpha+\beta(\frac{\Delta x}{\tau}+v_k)+\mathcal{E}(\frac{\Delta x}{\tau},-v_k,\nu)+\frac{E\Delta x}{\theta}\bar\rho\right] & = & f^n_j(-v_k), \end{array}\right\}$$

and with the same coefficients, the outgoing states $\tilde f_{j-\frac12}(\pm\mathbf{V})$ read:

$$\begin{array}{rcl} \tilde f_{j-\frac12}(v_k) & = & \mathcal{M}_\theta(v_k)\left[\alpha+\beta(\frac{\Delta x}{\tau}-v_k)+\mathcal{E}(\frac{\Delta x}{\tau},v_k,\nu)+\frac{E\Delta x}{\theta}\bar\rho\right], \\ \tilde f_{j-\frac12}(-v_k) & = & \mathcal{M}_\theta(-v_k)\left[\alpha+\beta v_k+\mathcal{E}(0,-v_k,\nu)\right]. \end{array}$$

Just recalling the matrix S_τ from (2.6), it boils down to:

$$\begin{pmatrix} \tilde f_{j-\frac12}(\mathbf{V})-\bar\rho\mathcal{M}_\theta(\mathbf{V})\frac{E\Delta x}{\theta} \\ \tilde f_{j-\frac12}(-\mathbf{V}) \end{pmatrix} = S_\tau \begin{pmatrix} f^n_j(\mathbf{V}) \\ f^n_{j+1}(-\mathbf{V})-\bar\rho\mathcal{M}_\theta(\mathbf{V})\frac{E\Delta x}{\theta} \end{pmatrix}. \tag{4.2}$$

The Godunov scheme (2.2)–(4.2) supplemented by a standard finite-differences Poisson solver for (1.2) is the algorithm which is used in [33] to obtain the numerical results of Fig. 11.5 (see page 229). Its large-time behavior is consistent with [11] but one drawback is that the electrons temperature remains too close to the lattice's θ.

4.2. Implementation of inflow Maxwellian boundary conditions. Realistic computations are carried out in a computational domain which is bounded in the space variable. In order to implement Maxwellian injection on the left/right boundaries within a well-balanced framework, one discretizes the left state (handling the right one is done similarly) as $f_{left}(\mathbf{V})=\rho_D(x_{left})\mathcal{M}_\theta(\mathbf{V})\in\mathbb{R}^K_+$. Without loss of generality, assume that $x_{left}=0$, C_0 is the "ghost cell" centered in $j=0$ so the interface with the first computational cell C_1 is $x_{\frac12}=\frac{\Delta x}{2}$. To advance in time the Godunov scheme (3.2), one needs "scattered boundary states" $\tilde f_{\frac12}(\mathbf{V})$, solutions of

$$\begin{pmatrix} \tilde f_{\frac12}(\mathbf{V})-\frac{E^n_{\frac12}\Delta x}{\theta}\bar\rho^n_{\frac12}\mathcal{M}_\theta(\mathbf{V}) \\ \tilde f_{\frac12}(-\mathbf{V}) \end{pmatrix} = S_\tau \begin{pmatrix} f_{left}(\mathbf{V}) \\ f^n_1(-\mathbf{V})-\frac{E^n_{\frac12}\Delta x}{\theta}\bar\rho^n_{\frac12}\mathcal{M}_\theta(-\mathbf{V}) \end{pmatrix},$$

where $E^n_{\frac12}=\frac{1}{\Delta x}(\varphi_{left}-\varphi^n_1)$. The K values $\tilde f_{\frac12}(-\mathbf{V})$ are useless. These boundary conditions are implemented in heavily doped regions (the source and the drain for a one-dimensional n^+nn^+ device) where the deviation from the normalized Maxwellian can be fairly considered small. Hence temperature jumps at borders remain small too. The uniform L^∞ bound in Proposition 1 cannot hold here because there is a net mass flow through both the boundaries until the macroscopic current becomes a constant in the whole computational domain, at steady-state [11].

5. Equilibration of a n^+nn^+ one-dimensional transistor. We display hereafter the behavior of these "scattering schemes" on elementary models of n^+nn^+ devices: the temperature is fixed to $\theta=\frac12$. The computational domain is $x\in(-1,1)$ (the depleted channel lies in the interval $x\in(-\frac12,\frac12)$) with inflow Maxwellian boundary conditions; it is coarsely gridded with 2^6 points so $\Delta x=2^{-5}$ and the CFL meets with Proposition 1: $\Delta t=0.95\Delta x/v_{MAX}$. A double Legendre Gaussian quadrature rule is applied for griding symmetrically the velocity variable with $v_{MAX}=2.8$. The numerical process we set up for these computations reads:

- in both highly doped zones (source and drain), the scheme (2.2)–(4.2),
- in the low-doped channel, the scheme (3.2)–(3.4) with the current fix (3.6).

We aim at checking the positivity-preserving properties and large-time stabilization arising from the standard choice of initial data induced by the doping profile:

$$f(t=0,x,v)=\rho_D(x)\mathcal{M}_\theta(v), \qquad x\in(-1,1).$$

The Figs. 5.1, 5.2, 5.4, 6.1, 6.2 display (left to right, top to bottom) the macroscopic density ρ, current J, temperature T, electric field E, kinetic density f in the x,v plane, and either various residuals decay (if zero bias is applied), or the macroscopic velocity u at numerical steady-state ($t\simeq 100$).

Parameter	Source	Channel	Drain
$\rho_D(x)$	1	0.02	1
$\tau(x)$	0.01	$+\infty$	0.01
$\lambda^2(x)$	0.15	0.5	0.15
θ	$\frac{1}{2}$	$\frac{1}{2}$	$\frac{1}{2}$

TABLE 5.1
Doping, relaxation time, scaled Debye length and lattice temperature for the "Schottky diode".

5.1. Well-balancing without collisions in the channel. We first want to display the behavior of the most elementary model where the linear Vlasov equation is set up in the device's channel, which is equivalent to let the collision rate diverge $\tau\to+\infty$. Vlasov equation describes ballistic charge transport, so such a model can be the one of a "metal-semiconductor" device, a Schottky junction. Hence, in the interval $x\in(-\frac{1}{2},\frac{1}{2})$, we simply use the scheme (3.2) with either the scattering matrix $\tilde{S}_E$ (see Lemma 2.2), or the Hamiltonian-Preserving one S_E with the current fix (3.6). Results at time $t=100$ are displayed in Fig. 5.1. One can see that the whole picture is completely symmetric around $x=0$, the macroscopic current is of the order to 10^{-8}, constant in the doped zones (source and drain) and monotone decreasing in the channel. The temperature is around 0.51 in the channel, 2% higher than the lattice's value θ. There is no collision process to tame the electric acceleration for $x\in(-\frac{1}{2},\frac{1}{2})$ in the presence of the other discontinuous parameters (see Table 5.1) hence this test-case is delicate to stabilize, despite its apparent simplicity.

Parameter	Source	Channel	Drain
$\rho_D(x)$	1	0.02	1
$\tau(x)$	0.01	1	0.01
$\lambda^2(x)$	0.05	0.5	0.05

TABLE 5.2
Doping values, relaxation time, scaled Debye length for a standard diode.

5.2. Steady-state balance with zero bias. Here we use a constant (non-zero) collision rate in the channel (see Table 5.2) and keep on working out numerically the case where a null bias is applied at the edges of the device. We must deal with another type of difficulty because, even if we have now a collision process in the channel to tame the Vlasov acceleration term, the simple Redheffer product (3.3) is by construction asymmetrical and leads, in large time, to the onset of a spurious current in the whole

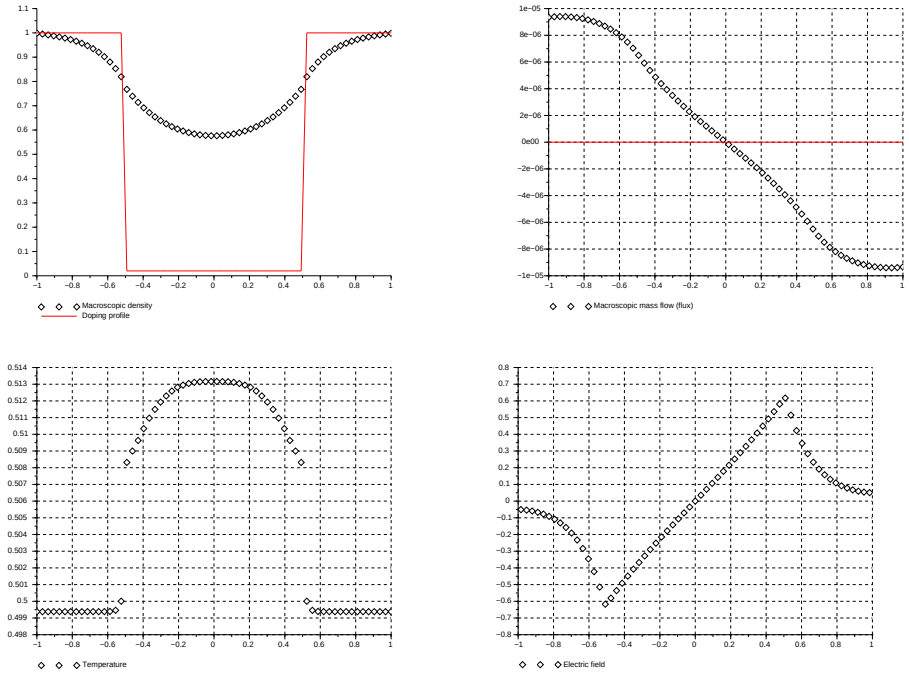

FIG. 5.1. *Steady-state at zero volt ($t = 100$) without collisions in the channel.*

device. Here, one aims at keeping as much as possible the symmetry of the initial data thus it is necessary to use the "Strang-type" star-product (3.4). Results at numerical steady-state, involving the current fix (3.6), are displayed on Fig. 5.2, where a small (spurious) current of the order of 10^{-9} appears again. The fact that these spurious currents are identical with and without collisions in the channel shows that, as soon as the star-product (3.4) is used, no worsening of large-time behavior appears despite handling a higher model complexity. The parameters $\tau, \lambda^2, \rho_D(x)$ are the same as the ones written in [33], Table 11.2; numerical results can be compared to what is displayed there, on Fig. 15.4, page 303. All considered quantities are very similar to the "high field scheme", except for the temperature, which appears much lower with the present algorithm. We don't have any rigorous explanation for this difference, especially because 3 schemes (well-balanced N-scheme [45], high-field WB of Chapter 15 [33], and the present one) yield 3 different temperatures.

We now define the so–called "Kullback-Leibler information",

$$\mathcal{K}(t,x) := \int_{\mathbb{R}} f(t,x,v) \log\left(\frac{f(t,x,v)}{\rho(t,x)\mathcal{M}_\theta(v)}\right) dv, \qquad x \in (-1,1),$$

which measures the loss of information when the distribution f is replaced by the simpler one $\rho(t,x)\mathcal{M}_\theta(v)$. The evolution in time of $\|\mathcal{K}(t,\cdot)\|_{L^1(-1,1)}$ corresponds to the red curve in the graphic, bottom right of Fig. 5.2, which is shown together with the L^2 residual on f (black curve), the H^1 semi-norm of J (green curve, $\|\partial_x J(t,\cdot)\|_{L^2(-1,1)}$) and the mass growth ($\|\rho(t,\cdot)\|_{L^1(-1,1)}$ blue curve). Residuals on f decrease monotonically, and total mass increases too. As expected, $\|\partial_x J(t,\cdot)\|_{L^2(-1,1)}$ decreases but slower than residuals (a plateau seems to exist around 10^{-2}). The L^1 norm of $\mathcal{K}(t,\cdot)$

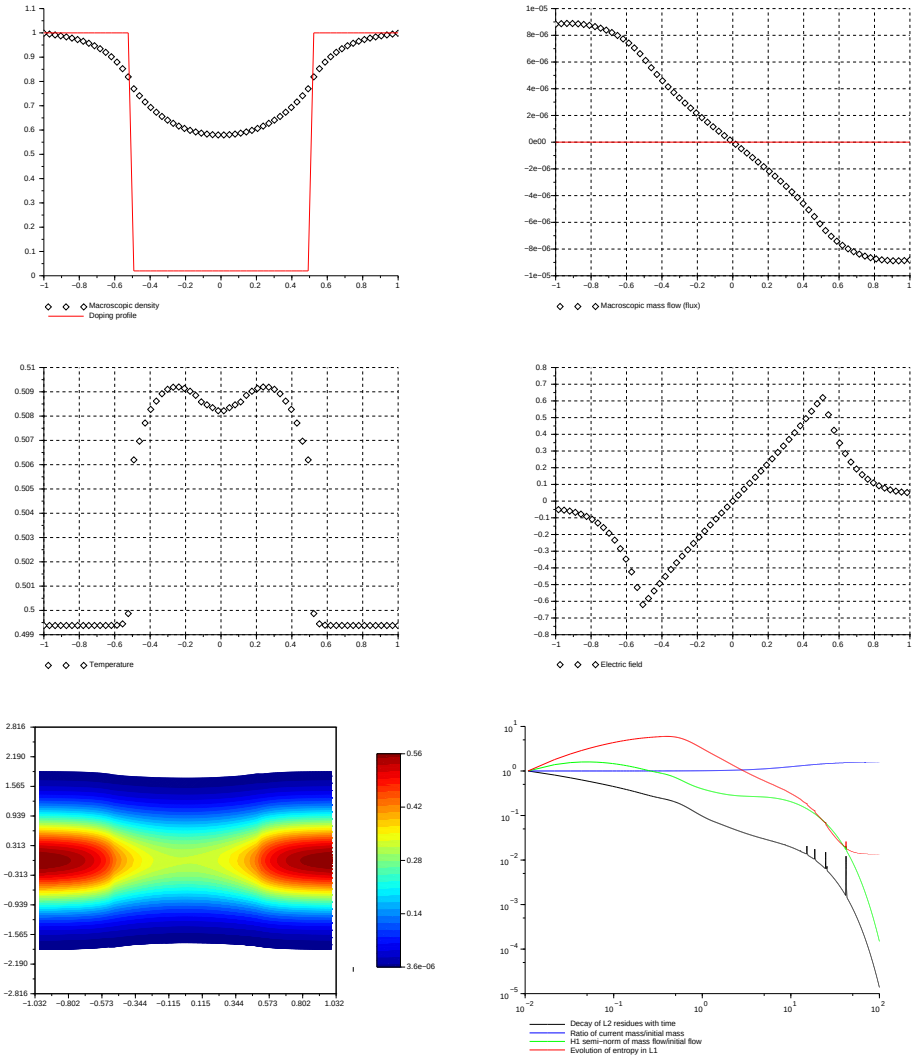

FIG. 5.2. *Steady-state at zero bias ($t = 100$) with constant collision rate in the channel.*

first grows as carriers begin to fill the channel, then decreases until it reaches a stable plateau: this indicates that close to each junction, the kinetic density f is quite different from a Maxwellian distribution, as signaled by the (small) temperature spikes. This feature was overlooked by a scheme proposed in [33]: see Figs. 11.5 and 11.7.

5.3. Flat currents with moderate bias. Now we aim at mimicking the test displayed in [33], Fig. 15.8 on page 308. A moderate bias $V = -\frac{1}{2}$ is imposed on the right side $x = 1$, and the device is expected to stabilize in large time onto a stationary regime endowed with a constant macroscopic current (which allows to stabilize the increase of the total mass contained in the device $\|\rho(t,\cdot)\|_{L^1}$). Results at $t = 100$ are displayed on Fig. 5.4, and again, what shows up first is the electrons temperature which is clearly lower than the ones obtained by means of both the "N-scheme" and the "high field scheme" which were set up in [33]. Besides, the (constant)

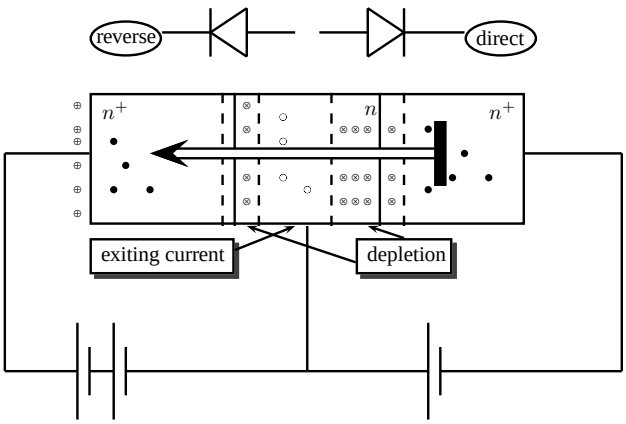

FIG. 5.3. *Schematic view of a transistor as 2 $p|n$ diodes: one directly polarized, one reversed.*

value of the current is very close to the most flat one in [33], and apart from the 2 small discontinuities at the junctions which appear with the "high field scheme", the macroscopic densities appear identical (and the electric fields too).

According to [35] (page 18) or [41], the length of a depletion layer around a $p|n$ junction scales with λ, the square root of the scaled Debye length. The parameters given in Table 5.2 indicate that the size of the depletion layer located around $x \simeq \mp\frac{1}{2}$, should be larger in the channel than in the doped areas (source or drain). This is well rendered as one can see looking at the electric field on Fig. 5.4: both spikes signal the electrostatic barriers arising from the equilibration of $p|n$ junctions, and they are supported in the depletion layers. For instance, the depletion layer of the directly polarized junction (see Fig. 5.3) around $x = -\frac{1}{2}$ starts at $x \simeq -0.9$ and ends at $x \simeq 0.2$: we have a depletion length of 0.4 in the source, and 0.7 in the channel. The one around $x = \frac{1}{2}$ runs from $x \simeq 0.3$ to $x = 1$. The resistance of a depletion layer grows with its length, hence we have a big current generated in the source, which carriers cannot recombine correctly in the channel. This is exactly what we want unless the transistor reduces just to an elementary $p|n$ diode with a lot of "exiting current". In order to recover a big current in the drain, one reverse-polarizes the second $p|n$ junction and sets up a strong potential drop (the forward bias $-|V|$): this reversed diode acts just as an anode which captures all the electrons, not recombined in the channel. A depletion layer can be thought of as an intrinsic semiconductor, hence ballistic transport of carriers is possible (thanks to Bloch theory) up to lattice vibrations which increase quickly with the temperature θ. Hence it would make sense to let the relaxation time τ, at least in the channel, grow with θ, too.

It is remarkable that the elementary kinetic model (1.1), (1.2) which doesn't contain any recombination/depletion information, succeeds in reproducing such a complex behavior, just relying on the self-consistent Poisson equation (1.2). The dynamics of this model (henceforth of the numerical scheme) are governed by:

- particles enter the computational domain through the ohmic contacts (1.3),
- they cannot settle in the doped areas because λ is low (quasi-neutrality),
- they accelerate and slowly fill in the channel (where λ is bigger) because they feel the anode's attraction (rendered by means of the forward bias) until a stable balance is reached with Poisson's self-consistent repulsive forces.

Hence the balancing effect of the scattering matrices is of critical importance as it is

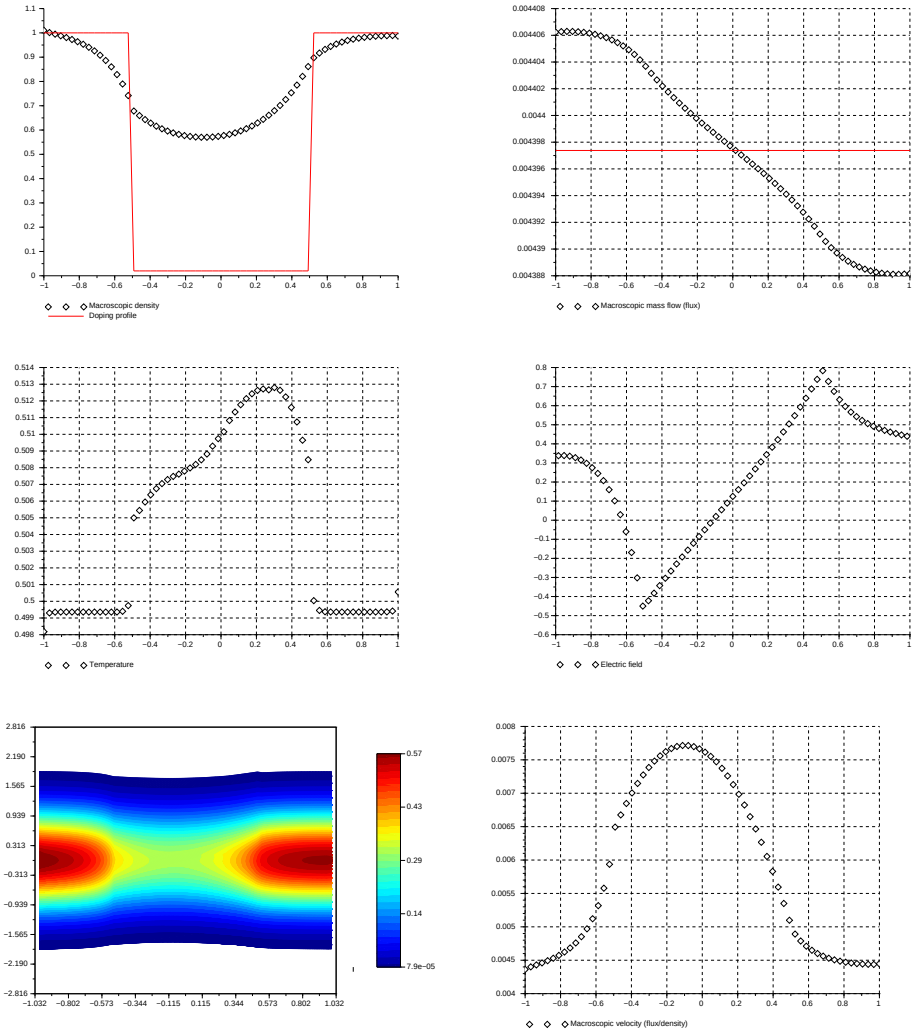

FIG. 5.4. *Steady-state at bias* $V = -\frac{1}{2}$ *(*$t = 100$*) with constant collision rate in the channel.*

the only effect still present in the kinetic model which is able to mimic the depletion layers. The net gain is that it suffices to run a simple model instead of simulating a more involved two-species equation endowed with a recombination process.

6. Velocity saturation with field-dependent relaxation time. It is stipulated, *e.g.* in [35] (see page 24), that in order to render a saturation effect, namely that the drift velocity and the collision rate must be bounded functions of the modulus of the electric field $|E|$ in order to prevent infinite values if $|E|$ becomes unbounded in the vicinity of transition points (junctions). This modification, leading to the well-known phenomenon of *velocity saturation* has 2 antagonistic outcomes:

- it tames even more the electric acceleration near the boundaries of the channel by strongly increasing the collision rate. Consequently, the possible "temperature spikes" are affected there too,

Parameter	Source	Channel	Drain
$\rho_D(x)$	1	0.02	1
$\tau(x,E)$	0.01	$\frac{1}{1+2\lvert E\rvert}$	0.01
$\lambda^2(x)$	0.015	0.05	0.015

TABLE 6.1
Doping values, relaxation time, scaled Debye length for the saturation diode.

- it worsens both the nonlinearity and the stiffness of the kinetic equation, thus numerically achieving a stationary balance between all these nonlinear terms becomes even more delicate.

Corresponding parameters are shown in Table 6.1 where the (discontinuous) Debye length was also decreased in order to decrease the possible mass inflow in the device before reaching steady-state. This choice increases the electric field around the junctions, thus makes the effect of the field-dependent collision rate more noticeable.

6.1. Zero bias with a regime close to quasi-neutrality. With respect to the values displayed in Figs. 5.1 and 5.2, one sees at once on Fig. 6.1 that now, the amplitude of the electric field's modulus has nearly been multiplied by 4. The greater difficulty in achieving a global balancing among all these nonlinear terms (acceleration and collisions) appears as the resulting numerical stationary current ceases to be monotone: however, the saturation process reduces the remaining spurious currents to an order of 10^{-9}, nearly identical than the ones appearing in the (less nonlinear) former cases. The steady-state macroscopic density is noticeably lower too, as an effect of the shorter Debye lengths (the electrons screening distance is bigger, hence self-consistent repulsive effects are stronger). Without any forward bias, the temperature in the channel is now 3% over the lattice's θ.

6.2. Applying a rather strong forward bias. Since we are closer to a regime of quasi-neutrality, it is necessary to apply stronger biases in order to create macroscopic currents in the device. Here we select $V = -\frac{3}{2}$, a value triple with respect to what was applied for generating the results of Fig. 5.4. The numerical stationary macroscopic current presents a deviation with respect to its arithmetical mean of the order of 10^{-8}, but it is strongly non-monotonic. Its value is around 0.0113, which is nearly the triple of the one showing up on Fig. 5.4, $\simeq 0.004$ (in spite of a higher value of ρ). This comes from the triple bias yielding local stiffness in the electric field. Temperatures in the channel are higher, too, but significantly lower compared to the ones computed in [33], Chapter 15. Clearly, being a moment of order 2, the temperature is a quantity sensitive to truncation errors (especially for high-velocity particles) as its computation also asks for both the macroscopic density and momentum,

$$T(t,x) = \int_{\mathbb{R}} \left(v - \frac{J(t,x)}{\rho(t,x)} \right)^2 f(t,x,v)dv, \quad J(t,x) = \int_{\mathbb{R}} v f(t,x,v)dv := \rho u(t,x),$$

with $u(t,x)$ the macroscopic velocity. Our WB schemes based on scattering S-matrices produce moments of order 0 and 1 which are quite insensitive to Δx, the grid size, but order 2 moments may still be considered as "fragile".

REMARK 4. *A field-dependent carriers mobility is meant to render the "pinch-off" of a depleted channel submitted to an excessive potential drop. Numerically, it is possible to see the saturating (stationary) currents as a function of the applied forward*

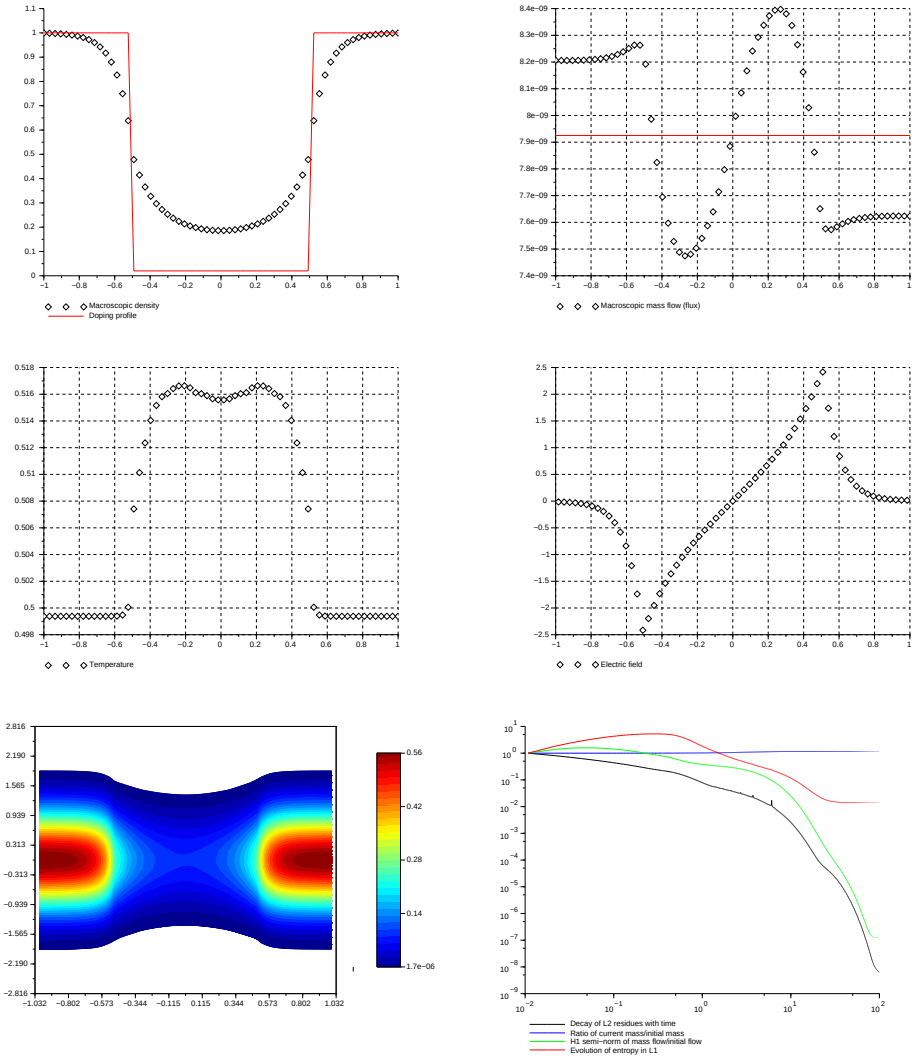

FIG. 6.1. *Steady-state at zero bias ($t = 100$) with field-dependent collision rate.*

bias: see Fig. 6.3. The straight line corresponds to the linear regression of currents generated with biases lower than 4, for which the device works purely as a resistor.

7. Conclusion. Finite volumes method is built to enforce mass conservation property (in opposition to finite elements). Well-balanced extensions aim at furnishing moreover qualitatively correct stationary mass flows too. Observe that an oscillating current arising close to the junctions indicates a poor resolution of the depletion layer, and is likely to produce a discrepancy on the resulting temperature as well.

Besides, it may be possible to perform an integration of the present methods, where numerical fluxes are based on S-matrices, inside the nowadays popular Discontinuous Galerkin algorithms [19] in order to raise up the overall accuracy. More involved kinetic models, where the inflow boundary value problem for the stationary equations cannot be easily solved, may seem difficult to handle by means of our present

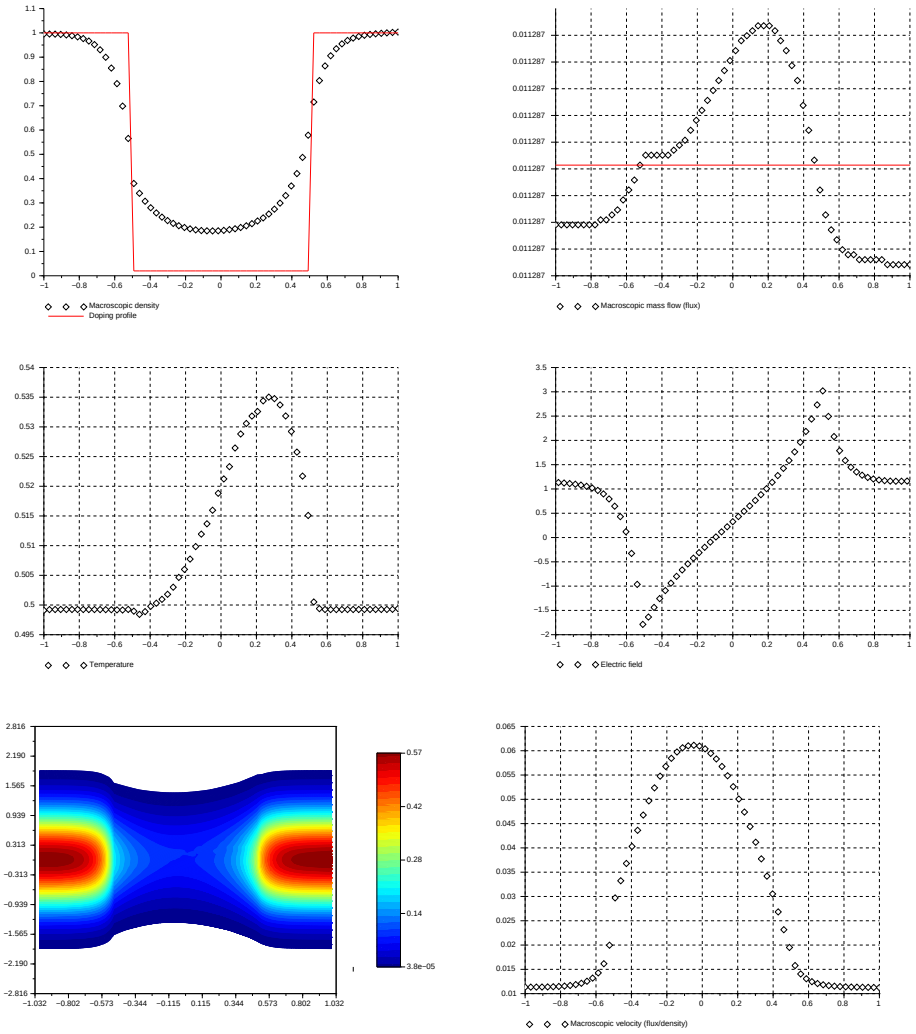

FIG. 6.2. *Steady-state at bias* $V = -\frac{3}{2}$ *(*$t = 100$*) with field-dependent collision rate.*

approach: in such cases, Bellman's Invariant imbedding theory [9], where scattering coefficients are derived by means of Ricatti differential equations, may help.

Appendix A. Weakly collisional Landau damping.

For the sake of completeness, we set up hereafter a benchmark already considered in [33], pages 225–227 and inspired by the theoretical calculations published in [22]. The computational domain is $x \in (-1, 1)$ with periodic boundary conditions; it is gridded with 2^7 points thus $\Delta x = 2^{-6}$. The initial data reads

$$f(t = 0, x, v) = \rho_0 \mathcal{M}_\theta(v)(1 + A\cos(2\pi x)), \qquad A = 0.15. \tag{A.1}$$

When set up with the ballistic Vlasov-Poisson equation, those initial data lead to the well-known phenomenon of *Landau damping*, that is to say a stable exponential decay of the electric field endowed with periodic oscillations. It turns out that this behavior

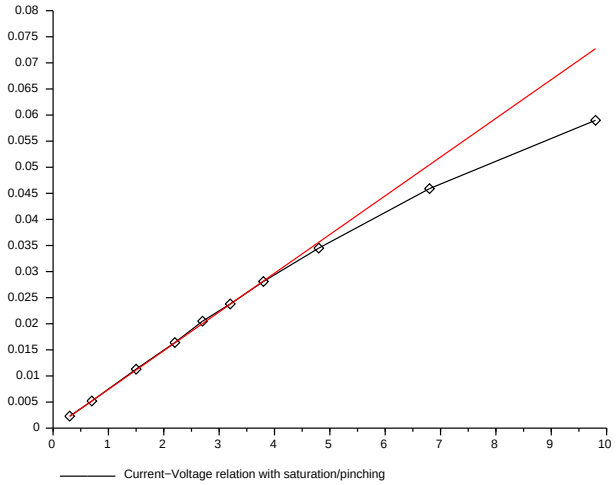

FIG. 6.3. *Current-Voltage relation showing linear resistor and saturating behavior.*

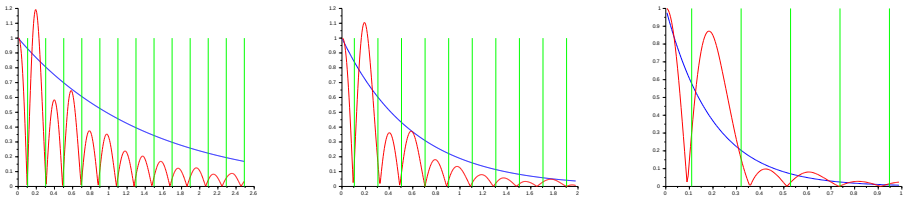

FIG. A.1. *Numerical decay w.r.t time of the average electric field for* $\tau = 0.7, 0.3, \frac{1}{10}$.

survives in the context of the collisional model (1.1)–(1.2) with constant parameters τ, λ and no doping profile, $\rho_D \equiv 0$. By defining the constant *plasma frequency* $\omega_P = \sqrt{\rho_0}$, *dielectric frequency* $\omega_D = \tau\rho_0$ and the thermal velocity $v_{th} = 2\sqrt{\theta}$, Degond and Guyot-Delaurens [22] derive the dispersion relation governing plane waves with frequency ω and wave vector k emerging from (A.1):

$$\begin{aligned} 0 = D(\omega, k; \tau) &= 1 - \frac{\omega_P^2}{k^2}\int_{\mathbb{R}} \frac{\max'(v)}{v-z}dv + \frac{i}{\tau k}\int_{\mathbb{R}} \frac{\max(v)}{v-z}dv \\ &\simeq 1 - \frac{i}{\tau k v_{th}}\left(\frac{v_{th}}{z}\right) - \frac{1}{k^2\lambda_0^2}\left(\frac{v_{th}}{z}\right)^2, \qquad \frac{v_{th}}{z} \to 0 \end{aligned}$$

where $\lambda_0 = \frac{v_{th}}{\omega_P}$. It corresponds to a damped oscillator which exhibits 2 different regimes depending on the location of τ is located with respect to the critical value:

$$2\omega_P\tau_c = 1 \Leftrightarrow \tau_c = \frac{1}{2\sqrt{\rho_0}}.$$

1. For $\tau < \tau_c$, the regime is strongly collisional and exponential decay of the perturbations occurs, quickly damping the kinetic density f. The asymptotic decay rate, as $\omega_P\tau \to 0$, is given by the dielectric frequency ω_D.
2. For $\tau > \tau_c$, the regime is weakly collisional and damped oscillations are observed on the average value (*i.e.* the Fourier component in $\xi = 0$) of the

electric field. The complex frequency satisfying $D(\omega, k; \tau) \simeq 0$ reads:

$$\omega = \omega_r + i\omega_i = \pm\omega_P \sqrt{1 - \frac{1}{(2\omega_P\tau)^2}} - \frac{i}{2\tau}.$$

Thus one can check numerically the half-period of the oscillations and the speed of decay, which should read $T_\tau = \frac{\pi}{\omega_r}$ and $\exp(-t/2\tau)$ respectively. This is what is displayed on Fig. A.1 for various values of the relaxation parameter τ: the numerical oscillations are superimposed with the theoretical half-periods and decay rates and a good match appears.

Acknowledgement. The author thanks Dr. Ch. Buet for having pointed out the relevance of stochastic matrices in the context of numerical "elementary solutions".

REFERENCES

[1] R.E. Aamodt, K.M. Case, *Useful identities for half-space problems in linear transport theory*, Ann. Physics **21** (1963) 284–301.

[2] L.V. Ballestra, R. Sacco, *Numerical problems in semiconductor simulation using the hydrodynamic model: a second-order finite difference scheme*. J. Comput. Phys. **195** (2004) 320–340.

[3] L.B. Barichello, M. Camargo, P. Rodrigues and C.E. Siewert, *Unified Solutions to Classical Flow Problems Based on the BGK Model*, ZAMP **52** (2001) 517-534.

[4] L.B. Barichello C.E. Siewert, *A discrete-ordinates solution for a non-grey model with complete frequency redistribution*, JQSRT **62** (1999) 665–675

[5] R.C. Barros, E.W. Larsen, *A Numerical Method for One-Group Slab-Geometry Discrete Ordinates Problems*, Nuclear Science and Engineering, 19-104 (1990), 199-208

[6] G.R. Bart, R.L. Warnock, *Linear integral equations of the third kind*, SIAM J. Math. Anal. **4** 609-622 (1973).

[7] R. Beals, *An abstract treatment of some forward-backward problems of transport and scattering*, J. Funct. Anal. **34** (1979) 1–20.

[8] P. Béchouche, L. Gosse, *A Semiclassical Coupled Model for the Transient Simulation of Semiconductor Devices*, SIAM J. Stat. Comput. **29** (2007) 376–396.

[9] R.E. Bellman, G.M. Wing, **An introduction to invariant imbedding**, SIAM Classics in Mathematics (1985).

[10] N. Ben Abdallah, *A Hybrid Kinetic-Quantum Model for Stationary Electron Transport* J. Stat. Phys. **90** 627-662, 1998.

[11] N. Ben Abdallah, J. Dolbeault, *Relative entropies for kinetic equations in bounded domains (irreversibility, stationary solutions, uniqueness)* Arch. Ration. Mech. Anal. **168** 253-298, 2003.

[12] N. Ben Abdallah, I. Gamba, A. Klar, *The Milne problem for high field kinetic equations* SIAM J. Applied Math. **64** 1739-1736, 2004.

[13] N. Ben Abdallah, M.L. Tayeb, *Diffusion Approximation for the one dimensional Boltzmann-Poisson system*, DCDS-B **4** 1129–1142 (2004).

[14] F. Bouchut, T. Morales, *A subsonic-well-balanced reconstruction scheme for shallow water flows*, SIAM J. Numer. Anal. **48** (2010) 1733–1758.

[15] J.A. Carrillo, I. Gamba, C.W. Shu, *Computational macroscopic approximations to the one-dimensional relaxation-time kinetic system for semiconductors* Physica D **146** (2000) 289–306.

[16] Kenneth M. Case, *Elementary solutions of the transport equation and their applications*, Ann. Physics **9** (1960) 1–23.

[17] K.M. Case, P.F. Zweifel, **Linear transport theory**, Addison-Wesley series in nuclear engineering (1967).

[18] C. Cercignani, *The method of elementary solutions for kinetic models with velocity dependent collision frequency*, Ann. Physics **40** (1966) 469.

[19] Y. Cheng, I.M. Gamba, J. Proft, *Positivity-preserving discontinuous Galerkin schemes for linear Vlasov-Boltzmann transport equations*, Math. Comput. **81** (2012), 153–190.

[20] N. Crouseilles, M. Lemou, An asymptotic preserving scheme based on a micro-macro decomposition for collisional Vlasov equations: Diffusion and high-field scaling limits, Kin. Rel. Models, 4 (2011), 441-477.
[21] Ch. Dalitz, *Half-space problem of the Boltzmann equation for charged particles*, J. Stat. Phys. **88**. (1997) 129–144.
[22] P. Degond, F. Guyot-Delaurens, *Particle Simulations of the Semiconductor Boltzmann Equation for One Dimensional Inhomogeneous Structures*, J. Comput. Phys. **90** (1990) 65–97.
[23] F. Delarue, F. Lagoutiere, *Probabilistic analysis of the upwind scheme for transport equations* Arch. Rat.l Mech. Anal. **199** (2011) 229-268.
[24] Dimarco, G., Pareschi, L., Rispoli, V. (2013). Implicit-Explicit Runge-Kutta schemes for the Boltzmann-Poisson system for semiconductors. arXiv preprint arXiv:1305.1759.
[25] N.J. Fisch, M. Kruskal, *Separating variables in two-way diffusion equations*, J. Math. Phys. **21** (1980) 740–750.
[26] Giovanni Frosali, Cornelius V. M. van der Mee, Stefano L. Paveri-Fontana, *Conditions for runaway phenomena in the kinetic theory of swarms*, J. Math. Phys. **30** (1989) 1177–1186.
[27] Frédérique Fuchs, *Asymptotic analysis of the degenerate Boltzmann-Poisson system for semiconductors*, Transp. Theo. Stat. Phys. **25** (1996) 151–173.
[28] J. Glimm, *The interaction of nonlinear hyperbolic waves*, Comm. Pure Appl. Math. **41** (1988), 569–590.
[29] J. Glimm, D. H. Sharp, *An S-matrix theory for classical nonlinear physics*. Found. Phys. **16** (1986) 125–141.
[30] L. Gosse, *Transient radiative transfer in the grey case: well-balanced and asymptotic-preserving schemes built on Case's elementary solutions*, J. Quant. Spectro. & Radiat. Transfer **112** (August 2011) 1995-2012.
[31] L. Gosse, *Well-balanced schemes using elementary solutions for linear models of the Boltzmann equation in one space dimension*, Kinetic Relat. Mod. **5** (2012) 283–323.
[32] L. Gosse, *A well-balanced scheme for kinetic models of chemotaxis derived from one-dimensional local forward-backward problems*, Math. Biosci. **242** (2013) 117–128.
[33] L. Gosse, **Computing Qualitatively Correct Approximations of Balance Laws**, Springer (2013) ISBN 978-88-470-2891-3
[34] C. Greengard, P. A. Raviart, *A boundary value problem for the stationary Vlasov-Poisson equations: The plane diode*, Comm. Pure Appl. Math. **43** (1990) 473–507.
[35] J.W. Jerome, **Analysis of Charge Transport: Mathematical Theory of Semiconductor Devices**, Springer (1996).
[36] S.Jin, L.Pareschi, *Discretization of the multiscale semiconductor Boltzmann equation by diffusive relaxation schemes*, J. Comput. Phys. 161, pp.312-330, (2000)
[37] Shi Jin, Xin Wen , *Hamiltonian-preserving schemes for the Liouville equation with discontinuous potentials*, Commun. Math. Sci. **3** (2005) 285–315.
[38] Ansgar Jüngel, **Transport Equations for Semiconductors**, Springer (2009).
[39] H. G. Kaper, C.G. Lekkerkerker, J. Hejtmanek, **Spectral Methods in Linear Transport Theory**, Birkhäuser (1982).
[40] T. Lu, S. Shiou, *Inverses of* 2×2 *block matrices*, Comput. & Math. Applic. 43 (2002) 119–129.
[41] P.A. Markowich, C.A. Ringhofer, C. Schmeiser, **Semiconductor equations**. Springer, 1990.
[42] S.L. Paveri-Fontana, C. V. M. van der Mee, P. F. Zweifel, *A Neutral Gas Model for Electron Swarms*, J. Stat. Phys. **83** (1999) 247–265
[43] R. Redheffer, *Difference equations and functional equations in transmission-line theory*, Modern Mathematics for the Engineer, E. F. Beckenbach, ed., Vol. 12, 282–337, McGraw-Hill, New York, 1961
[44] R. Redheffer, *On the relation of transmission-line theory to scattering and transfer*, J. Math. and Phys. 41 (1962) 1–41
[45] Roe, P. L., Sidilkover, D. (1992). *Optimum positive linear schemes for advection in two and three dimensions*. SIAM journal on numerical analysis, 29(6), 1542-1568.
[46] G. Salton, *The Use of the Central Limit Theorem for Interpolating in Tables of Probability Distribution Functions*, Math. Tables and Other Aids to Computation **13** (1959) 213–216.
[47] C.E. Siewert, S.J. Wright, *Efficient eigenvalue calculations in radiative transfer*, J. Quant. Spectro. Radiat. Transf. (1999) 685–688.
[48] Dan Timotin, *Redheffer products and characteristic functions*. J. Math. Anal. Applic. **196** (1995) 823–840.
[49] C. Toepffer, C. Cercignani, *Analytical results for the Boltzmann equation*, Contrib. Plasma Phys. (1999) **37** (1997) 279–291.
[50] X. Wen, S. Jin, *The* L^1*-Error Estimates for a Hamiltonian-Preserving Scheme for the Liouville Equation with Piecewise Constant Potentials*, SIAM J. Numer. Anal.**46** (2008) 2688–2714